SCIENCE CHINA
Information Sciences

• RESEARCH PAPER •

November 2018, Vol. 61 112207:1–112207:16
https://doi.org/10.1007/s11432-017-9434-7

Multivariable sliding mode backstepping controller design for quadrotor UAV based on disturbance observer

Zheng ZHANG[1], Fang WANG[1*], Ying GUO[1] & Changchun HUA[2]

[1]*School of Science, Yanshan University, Qinhuangdao* 066004*, China;*
[2]*School of Electric Engineering, Yanshan University, Qinhuangdao* 066004*, China*

Received 21 October 2017/Revised 24 January 2018/Accepted 2 April 2018/Published online 17 October 2018

Abstract This paper deals with the tracking control problem of quadrotor unmanned aerial vehicles (QUAVs) with external disturbances. First, because the QUAV model contains two non-integrity constraints, the dynamic model of the QUAV is decomposed into two subsystems which are independently controlled, so as to reduce controller design complexity. Secondly, the nonlinear disturbance observer (DOB) technique is integrated into a backstepping control method to design the controller for the first subsystem, in which a DOB is applied to estimate the lumped uncertainty. Based on the double power reaching law and the DOB, a multivariable sliding mode control (MSMC) scheme is developed for the second subsystem. Thirdly, based on Lyapunov theory, the closed-loop system is proved to be asymptotically stable. Finally, our comparative simulation results demonstrate that the presented control scheme behaves better in terms of tracking performance than the adaptive backstepping control (ABC) approach.

Keywords quadrotor unmanned aerial vehicle, QUAV, nonlinear DOB, backstepping control, sliding mode control, power reaching law

Citation Zhang Z, Wang F, Guo Y, et al. Multivariable sliding mode backstepping controller design for quadrotor UAV based on disturbance observer. Sci China Inf Sci, 2018, 61(11): 112207, https://doi.org/10.1007/s11432-017-9434-7

1 Introduction

Quadrotor unmanned aerial vehicles (QUAVs) have many advantages over traditional helicopters because of their vertical flying, hovering, and smaller diameter characteristics. They qualify for mapping, surveillance, inspection, and rescue missions [1–3]. They have recently been receiving increasing attention.

Controller design for QUAVs is very challenging because of their heavy couplings and parameter uncertainties. Many literatures [4–8] focus on the modeling and controlling of UAV, and researchers have achieved good QUAV performances. The linear control techniques have been successfully applied for UAV control system design [9–12], such as PID control, PD control, and the H_∞ control method. However, in the absence of nominal operating conditions, linear controllers cannot provide good flight performance. To solve this problem, nonlinear control techniques, such as the backstepping control method and the sliding mode control method, have been proposed for UAV controller design in [13–17]. In [16], a backstepping control scheme was developed to achieve stable tracking for the desired position and yaw angle of an unmanned aerial vehicle (UAV). Additionally, a linear tracking differentiator was integrated with a

* Corresponding author (email: wangfang@ysu.edu.cn)

command-filtered backstepping technique to design a trajectory-tracking controller for a UAV in [17]. A robust nonlinear controller design approach was shown to achieve trajectory tracking for a QUAV in [18]. In order to solve the multi-UAV formation reconfiguration problem, a hybrid particle swarm optimization and genetic algorithm was proposed in [19]. Though the desired tracking performance for the UAVs was achieved, parametric uncertainties and aerodynamic effects were not taken into account in [13–17]. Then, in [20], an adaptive control strategy based on Lyapunov theory was proposed for UAVs, while taking parameter uncertainties into consideration. Moreover, in [21], an adaptive backstepping control scheme was designed for UAVs under sensor and actuator failure effects. However, it should be pointed out that external disturbances were not considered in [20, 21] at the control design level.

For UAVs, when parameter uncertainties and external disturbances are considered, the designed control system must behave robustly to handle them. The sliding mode control (SMC) technique was one of the most robust and effective methods used to deal with uncertainty in [22–24]. Because of its insensitivity to parametric uncertainties, model errors, and other uncertainties, the first adaptive multivariable finite-time control algorithm based on SMC was developed in [25] for attitude control of a UAV, where an excellent tracking performance was achieved using the developed algorithm. Subsequently, multivariable finite-time control algorithms were proposed in [26, 27] for tracking control of UAVs. In addition, a multivariable super-twisting algorithm-based SMC method and a novel sliding mode controller were designed respectively for small unmanned helicopters and small-scale unmanned helicopters with mismatched uncertainty in [28, 29]. The compounded disturbances were estimated by the sliding mode observer. In [28], a disturbance-observer-based (DOB-based) controller was designed based on multivariable super twisting and backstepping control to obtain robust trajectory tracking performance. In [29], a novel SMC strategy was proposed, in which an enhanced DOB was used to deal with the tracking control problem of UAVs with mismatched uncertainty. An adaptive SMC control scheme was proposed for UAV systems with parametric uncertainties in [30]. Moreover, an SMC system was used for the stabilization problem of UAVs in [31]; however, the chattering problem of traditional SMCs was not solved. Additional work about the application of SMCs for flight control can be found in [32, 33]. Although the backstepping technique is one of the most efficient techniques proposed for nonlinear systems and has been employed in engineering fields in [34–36], it cannot guarantee asymptotic convergence in the presence of external disturbances. Thus, it is often combined with other technologies to achieve a better control performance. A flight control law based on a sensor-based backstepping technique for UAVs was proposed in [37]. An adaptive backstepping control scheme was designed for mixed QUAVs in [38], and, based on an adaptive SMC control method, a backstepping control scheme was derived for UAV attitude control in [39]. A radial basis function neural network (RBFNN) was combined with an adaptive backstepping control method to design a controller for a model-scale helicopter in [40]. The DOB technique has been applied as a compensator to effectively suppress unknown uncertainties and external disturbances. It does not rely on the system's mathematical model, and it can be used to estimate the external disturbances of the controlled object in real time and actively compensate for a limited period of time, as demonstrated in [41]. Thus, it has been used in the tracking control problem of UAVs in [42, 43]. A linear dual DOB control scheme was proposed to improve the trajectory tracking precision of a QUAV with external disturbances in [42]. Considering the external disturbances and input delays, a DOB based on the backstepping control scheme was designed in [43]. In these control strategies, the DOB was used as a compensator to effectively suppress external disturbances.

Motivated by aforementioned studies, in this paper, the disturbance observer and SMC methods are integrated with a backstepping control scheme to design a controller for a QUAV. The contributions of this paper can be summarized as follows. First, because the QUAV model contains two non-integrity constraints, the model of our QUAV is divided into two subsystems to reduce controller design complexity. Secondly, a DOB-based backstepping controller is designed for the first subsystem, while a double power reaching law SMC based on a DOB is developed for the second subsystem. At the control design level, the DOB is employed to handle the lumped uncertainty, and the estimated error of the disturbance observer is used to achieve stability. A first-order filter is used to eliminate the problem of "explosion of terms" at the control design level of the first subsystem. Finally, comparative simulations between the designed control method and the adaptive backstepping control (ABC) approach are carried out to show that the designed control scheme achieves a better control performance than the ABC strategy.

The remaining parts of this paper are organized as follows. In Section 2, a QUAV model and a description of the problem are presented. The controller design is shown in Section 3, and a stability analysis is presented in Section 4. Then, our simulation results are shown in Section 5. Finally, our conclusion is provided in Section 6.

2 QUAV model and problem description

The four rotors of a QUAV are symmetrically distributed in four directions emerging from its body, and the movement of a QUAV is obtained by changing the lift generated by appropriately adjusting the rotational speeds of the four rotors [44].

The dynamic model of a QUAV is described by the following equations [31, 45]:

$$
\begin{aligned}
\ddot{x} &= \frac{1}{m}(\cos\phi\sin\theta\cos\psi + \sin\phi\sin\psi)u_1 - \frac{G_1\dot{x}}{m},\\
\ddot{y} &= \frac{1}{m}(\cos\phi\sin\theta\sin\psi - \sin\phi\cos\psi)u_1 - \frac{G_2\dot{y}}{m},\\
\ddot{z} &= \frac{1}{m}(\cos\phi\cos\theta)u_1 - g - \frac{G_3\dot{z}}{m},\\
\ddot{\phi} &= \frac{a}{J_{xx}}u_2 - \frac{G_4 a}{J_{xx}}\dot{\phi},\\
\ddot{\theta} &= \frac{a}{J_{yy}}u_3 - \frac{G_5 a}{J_{yy}}\dot{\theta},\\
\ddot{\psi} &= \frac{a}{J_{zz}}u_4 - \frac{G_6 a}{J_{zz}}\dot{\psi},
\end{aligned}
\tag{1}
$$

where x, y, z denote the position of the QUAV, and ϕ, θ, ψ denote the attitude of the QUAV. m, a are the quality of the quadrotor and the length of the wings, respectively. J_{xx}, J_{yy}, J_{zz} represent the inertia of the aircraft on the x, y, z axes, respectively. G_i $(i = 1, \ldots, 6)$ are the drag coefficients of the system. u_1, u_2, u_3, u_4 are the four control variables to be designed in the next section, and the relationship between them and the lift of the QUAV is

$$
\begin{aligned}
u_1 &= F_1 + F_2 + F_3 + F_4,\\
u_2 &= a(-F_2 + F_4),\\
u_3 &= a(-F_1 + F_3),\\
u_4 &= A(-F_1 + F_2 - F_3 + F_4),
\end{aligned}
\tag{2}
$$

where A represents the scale factor between lift and yaw torque, and F_1, F_2, F_3, F_4 are the lifts of the four rotors.

It can be seen from the QUAV dynamic model presented in (1) that the number of degrees of freedom is higher than the independent control inputs, and that the system is underactuated and heavily coupled. Additionally, because the system states are relatively independent, the system can be decomposed into two subsystems which can be controlled independently. In order to facilitate controller design, Eq. (1) can be expressed as follows:

$$
\Sigma_1 : \begin{cases}
\dot{\boldsymbol{x}}_1 = \boldsymbol{x}_2,\\
\dot{\boldsymbol{x}}_2 = \boldsymbol{R}_2\boldsymbol{x}_2 + \boldsymbol{S}_2\boldsymbol{x}_3 + \boldsymbol{D}_1,\\
\dot{\boldsymbol{x}}_3 = \boldsymbol{S}_3\boldsymbol{x}_4,\\
\dot{\boldsymbol{x}}_4 = \boldsymbol{R}_4\boldsymbol{x}_4 + \boldsymbol{S}_4\boldsymbol{U}_1 + \boldsymbol{D}_2,
\end{cases}
\tag{3}
$$

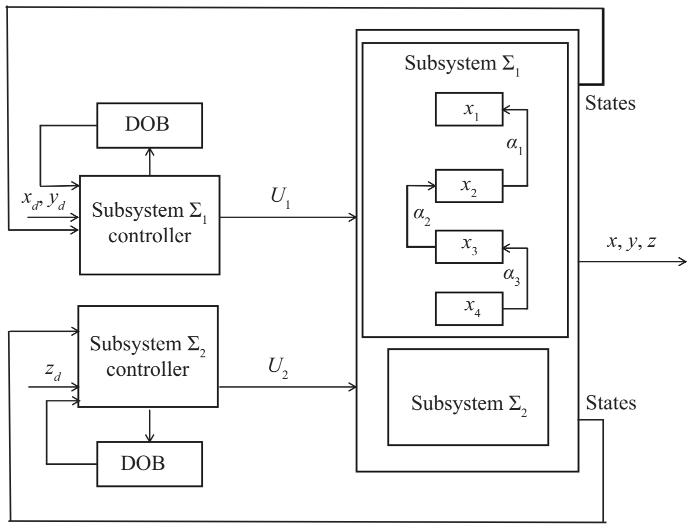

Figure 1 Architecture of the proposed control scheme.

$$\Sigma_2 : \begin{cases} \dot{\boldsymbol{x}}_5 = \boldsymbol{x}_6, \\ \dot{\boldsymbol{x}}_6 = \boldsymbol{R}_6\boldsymbol{x}_6 + \boldsymbol{S}_6\boldsymbol{U}_2 + \boldsymbol{F}_6 + \boldsymbol{D}_3, \end{cases} \tag{4}$$

where (3) is the underactuated subsystem Σ_1, and Eq. (4) is the fully actuated subsystem Σ_2. $\boldsymbol{D}_1, \boldsymbol{D}_2$ denote the external disturbances of Σ_1. $\boldsymbol{D}_3$ denotes the perturbation in subsystem Σ_2. The state variables and coefficient matrixes in Σ_1 and Σ_2 can be expressed as follows:

$$\boldsymbol{x}_1 = \begin{bmatrix} x \\ y \end{bmatrix}, \ \boldsymbol{x}_2 = \begin{bmatrix} \dot{x} \\ \dot{y} \end{bmatrix}, \ \boldsymbol{x}_3 = \begin{bmatrix} \sin\theta \\ \sin\phi \end{bmatrix}, \ \boldsymbol{x}_4 = \begin{bmatrix} \dot{\theta} \\ \dot{\phi} \end{bmatrix}, \ \boldsymbol{x}_5 = \begin{bmatrix} z \\ \psi \end{bmatrix}, \ \boldsymbol{x}_6 = \begin{bmatrix} \dot{z} \\ \dot{\psi} \end{bmatrix}, \ \boldsymbol{F}_6 = \begin{bmatrix} -g \\ 0 \end{bmatrix},$$

$$\boldsymbol{S}_2 = \frac{u_1}{m}\begin{bmatrix} \cos\phi\cos\psi & \sin\psi \\ \cos\phi\sin\psi & -\cos\psi \end{bmatrix}, \ \boldsymbol{S}_3 = \begin{bmatrix} \cos\theta & 0 \\ 0 & \cos\phi \end{bmatrix}, \ \boldsymbol{S}_4 = \begin{bmatrix} \frac{a}{J_{yy}} & 0 \\ 0 & \frac{a}{J_{xx}} \end{bmatrix}, \ \boldsymbol{S}_6 = \begin{bmatrix} \frac{\cos\phi\cos\theta}{m} & 0 \\ 0 & \frac{a}{J_{zz}} \end{bmatrix},$$

$$\boldsymbol{D}_1 = \begin{bmatrix} \Delta_x \\ \Delta_y \end{bmatrix}, \boldsymbol{D}_2 = \begin{bmatrix} \Delta_\theta \\ \Delta_\phi \end{bmatrix}, \boldsymbol{D}_3 = \begin{bmatrix} \Delta f_z \\ \Delta f_\psi \end{bmatrix}, \boldsymbol{R}_2 = -\begin{bmatrix} \frac{G_1}{m} & 0 \\ 0 & \frac{G_2}{m} \end{bmatrix}, \boldsymbol{R}_4 = \begin{bmatrix} \frac{-G_5 a}{J_{yy}} & 0 \\ 0 & \frac{-G_4 a}{J_{xx}} \end{bmatrix}, \boldsymbol{R}_6 = \begin{bmatrix} \frac{-G_3}{m} & 0 \\ 0 & \frac{-G_6 a}{m} \end{bmatrix}.$$

The control objective of this paper is to design a controller for the system described by (1) to make x, y, z track their reference commands x_d, y_d, z_d with external disturbances $\boldsymbol{D}_1, \boldsymbol{D}_2, \boldsymbol{D}_3$. Thus, the system is transformed into the following control objective: for subsystems Σ_1 and Σ_2, the designed control strategy makes $\boldsymbol{x}_1, \boldsymbol{x}_5$ track their reference commands $\boldsymbol{x}_{1d}, \boldsymbol{x}_{5d}$.

3 DOB-based control system design

In this section, a controller is developed for the QUAV to track the reference commands in the presence of external disturbances $\boldsymbol{D}_1, \boldsymbol{D}_2, \boldsymbol{D}_3$. The control architecture is shown in Figure 1.

As shown in Figure 1, the control inputs are designed for subsystems Σ_1 and Σ_2. For subsystem Σ_1, position x, y is controlled by the actual control input $\boldsymbol{U}_1$, which is designed by integrating the DOB with a backstepping control method. More precisely, $\boldsymbol{x}_1$ is controlled via the virtual control input α_1, $\boldsymbol{x}_2$ is controlled via the virtual control input α_2, $\boldsymbol{x}_3$ is controlled via the virtual control input α_3, and $\boldsymbol{x}_3$ is controlled via the actual control input $\boldsymbol{U}_1$. At the control design level, the DOB is used to estimate the lumped uncertainties $\boldsymbol{D}_1, \boldsymbol{D}_2$. Furthermore, for subsystem Σ_2, controller $\boldsymbol{U}_2$ is designed by combining the DOB and the sliding mode control method, in which the DOB is used to estimate the lumped uncertainty $\boldsymbol{D}_3$.

Before designing the controller, the following assumptions are made for disturbances $\boldsymbol{D}_i\,(i = 1, 2, 3)$, which are used during controller design and our stability analysis.

Assumption 1. The reference commands $\boldsymbol{x}_{1d}, \boldsymbol{x}_{5d}$ are continuous and differentiable.

Assumption 2. The disturbances change slowly, i.e., $\dot{\boldsymbol{D}}_i \approx [0\ \ 0]^{\mathrm{T}}$.

An estimation of $\boldsymbol{D}_i$ is made by the DOB, and is defined as $\hat{\boldsymbol{D}}_i$. The estimate error is

$$\tilde{\boldsymbol{D}}_i = \boldsymbol{D}_i - \hat{\boldsymbol{D}}_i. \tag{5}$$

Based on these assumptions and subsystem Σ_1, a backstepping control scheme is designed based on the DOB for subsystem Σ_1.

3.1 Subsystem Σ_1 controller design

In this subsection, the controller design for subsystem Σ_1 is explained. Because Σ_1 behaves in a strict feedback form with mismatched uncertainty, the backstepping control approach is applicable, and the DOB is employed to estimate the lumped uncertainty. The controller design for subsystem Σ_1 includes four steps; virtual control inputs are developed during the first three steps, and the actual control input is designed in the last step. The time derivatives of the virtual control inputs in the backstepping design procedure are estimated by the filter, so as to eliminate the problem of explosion of terms.

Step 1. Design of virtual control input α_1.

The tracking error of $\boldsymbol{x}_1$ is defined as

$$\boldsymbol{z}_1 = \boldsymbol{x}_1 - \boldsymbol{x}_{1d}, \tag{6}$$

where vector $\boldsymbol{x}_{1d}$ is the reference command.

We chose the following Lyapunov function:

$$V_1 = \frac{1}{2}\boldsymbol{z}_1^{\mathrm{T}}\boldsymbol{z}_1. \tag{7}$$

From (3) and (6), the time derivative of V_1 is

$$\dot{V}_1 = \boldsymbol{z}_1^{\mathrm{T}}(\boldsymbol{z}_2 + \alpha_1 - \dot{\boldsymbol{x}}_{1d}). \tag{8}$$

The error signal of $\boldsymbol{x}_2$ is defined as

$$\boldsymbol{z}_2 = \boldsymbol{x}_2 - \alpha_1, \tag{9}$$

where α_1 is the reference signal of $\boldsymbol{x}_2$.

From (8), virtual control input α_1 is designed as

$$\alpha_1 = \dot{\boldsymbol{x}}_{1d} - k_1\boldsymbol{z}_1, \tag{10}$$

and after substituting (10) into (8), we obtain

$$\dot{V}_1 = -k_1\boldsymbol{z}_1^{\mathrm{T}}\boldsymbol{z}_1 + \boldsymbol{z}_1^{\mathrm{T}}\boldsymbol{z}_2. \tag{11}$$

Step 2. Design of virtual control input α_2.

We chose the following Lyapunov function:

$$V_2 = \frac{1}{2}\boldsymbol{z}_2^{\mathrm{T}}\boldsymbol{z}_2 + V_1. \tag{12}$$

From (3), (10)–(12), the time derivative of V_2 becomes

$$\dot{V}_2 = \boldsymbol{z}_2^{\mathrm{T}}\boldsymbol{R}_2\boldsymbol{x}_2 + \boldsymbol{z}_2^{\mathrm{T}}\boldsymbol{S}_2(\boldsymbol{x}_3 - \alpha_{2d}) + \boldsymbol{z}_2^{\mathrm{T}}\boldsymbol{S}_2\alpha_{2d} + \boldsymbol{z}_2^{\mathrm{T}}\boldsymbol{D}_1 - \boldsymbol{z}_2^{\mathrm{T}}\dot{\alpha}_1 - k_1\boldsymbol{z}_1^{\mathrm{T}}\boldsymbol{z}_1 + \boldsymbol{z}_1^{\mathrm{T}}\boldsymbol{z}_2, \tag{13}$$

where variable α_{2d} is obtained by the filter. Then, the error signal of $\boldsymbol{x}_3$ is defined as

$$\boldsymbol{z}_3 = \boldsymbol{x}_3 - \alpha_2, \tag{14}$$

where α_2 is the reference signal of $\boldsymbol{x}_3$.

For disturbance $\boldsymbol{D}_1$, the following DOB is employed to estimate it [46]:

$$\begin{cases} \hat{\boldsymbol{D}}_1 = \boldsymbol{T}_1 + Q(\boldsymbol{x}_2), \\ \dot{\mathbf{T}}_1 = L(\boldsymbol{x}_2)\{-\boldsymbol{R}_2\boldsymbol{x}_2 - \boldsymbol{S}_2\boldsymbol{x}_3 - [\boldsymbol{T}_1 + Q(\boldsymbol{x}_2)]\}, \end{cases} \tag{15}$$

where

$$Q(\boldsymbol{x}_2) = \begin{bmatrix} \mu_1(\dot{x}^{\varepsilon_1} + \dot{x}^{\varepsilon_1}/\varepsilon_1) \\ \mu_2(\dot{y}^{\varepsilon_2} + \dot{y}^{\varepsilon_2}/\varepsilon_2) \end{bmatrix}, \quad L(\boldsymbol{x}_2) = \frac{\partial Q(\boldsymbol{x}_2)}{\partial \boldsymbol{x}_2} = \begin{bmatrix} \mu_1(1+\dot{x}^{\varepsilon_1-1}) & 0 \\ 0 & \mu_2(1+\dot{y}^{\varepsilon_2-1}) \end{bmatrix}, \quad \mu_i > 0,$$

and ε_j $(i = 1, 2; j = 1, 2)$ is a positive odd constant.

Based on (13) and (15), virtual control input α_2 is designed as

$$\alpha_2 = \boldsymbol{S}_2^{-1}(\dot{\alpha}_1 - \boldsymbol{z}_1 - k_2\boldsymbol{z}_2 - \boldsymbol{R}_2\boldsymbol{x}_2 - \hat{\boldsymbol{D}}_1). \tag{16}$$

The following filter is designed to estimate α_2,

$$\dot{\alpha}_{2d} = \frac{-(\alpha_{2d} - \alpha_2)}{\tau_1}, \tag{17}$$

where τ_1 is a positive constant, and the filter estimate error is defined as

$$\boldsymbol{e}_{2d} = \alpha_{2d} - \alpha_2. \tag{18}$$

From (14), (16) and (18), Eq. (13) yields

$$\dot{V}_2 = -k_1\boldsymbol{z}_1^{\mathrm{T}}\boldsymbol{z}_1 - k_2\boldsymbol{z}_2^{\mathrm{T}}\boldsymbol{z}_2 + \boldsymbol{z}_2^{\mathrm{T}}\boldsymbol{S}_2\boldsymbol{z}_3 - \boldsymbol{z}_2^{\mathrm{T}}\boldsymbol{S}_2\boldsymbol{e}_{2d} + \boldsymbol{z}_2^{\mathrm{T}}\tilde{\boldsymbol{D}}_1. \tag{19}$$

Step 3. Design of virtual control input α_3.

We chose the following Lyapunov function:

$$V_3 = \frac{1}{2}\boldsymbol{z}_3^{\mathrm{T}}\boldsymbol{z}_3 + V_2. \tag{20}$$

Based on (14) and (19), the time derivative of V_3 satisfies

$$\begin{aligned} \dot{V}_3 = &-k_1\boldsymbol{z}_1^{\mathrm{T}}\boldsymbol{z}_1 - k_2\boldsymbol{z}_2^{\mathrm{T}}\boldsymbol{z}_2 + \boldsymbol{z}_2^{\mathrm{T}}\boldsymbol{S}_2\boldsymbol{z}_3 - \boldsymbol{z}_2^{\mathrm{T}}\boldsymbol{S}_2\boldsymbol{e}_{2d} + \boldsymbol{z}_2^{\mathrm{T}}\tilde{\boldsymbol{D}}_1 \\ &+\boldsymbol{z}_3^{\mathrm{T}}\boldsymbol{S}_3(\boldsymbol{x}_4 - \alpha_{3d}) + \boldsymbol{z}_3^{\mathrm{T}}(\dot{\alpha}_2 - k_3\boldsymbol{z}_3 - \boldsymbol{z}_2^{\mathrm{T}}\boldsymbol{S}_2) - \boldsymbol{z}_3^{\mathrm{T}}\dot{\alpha}_2. \end{aligned} \tag{21}$$

The new variable α_{3d} is obtained by the filter. Then, the error signal of $\boldsymbol{x}_4$ is defined as

$$\boldsymbol{z}_4 = \boldsymbol{x}_4 - \alpha_3, \tag{22}$$

where α_3 is the reference signal of $\boldsymbol{x}_4$.

Virtual control input α_3 is designed as

$$\alpha_3 = \boldsymbol{S}_3^{-1}(\dot{\alpha}_{2d} - k_3\boldsymbol{z}_3 - \boldsymbol{z}_2^{\mathrm{T}}\boldsymbol{S}_2). \tag{23}$$

The following filter is applied to estimate α_3:

$$\dot{\alpha}_{3d} = \frac{-(\alpha_{3d} - \alpha_3)}{\tau_2}, \tag{24}$$

where τ_2 is a positive constant, and the filter estimate error is defined as

$$\boldsymbol{e}_{3d} = \alpha_{3d} - \alpha_3. \tag{25}$$

From (22), (23), and (25), Eq. (21) becomes

$$\dot{V}_3 = -k_1\boldsymbol{z}_1^{\mathrm{T}}\boldsymbol{z}_1 - k_2\boldsymbol{z}_2^{\mathrm{T}}\boldsymbol{z}_2 - k_3\boldsymbol{z}_3^{\mathrm{T}}\boldsymbol{z}_3 + \boldsymbol{z}_2^{\mathrm{T}}\tilde{\boldsymbol{D}}_1 + \boldsymbol{z}_3^{\mathrm{T}}\boldsymbol{S}_3\boldsymbol{z}_4 - \boldsymbol{z}_2^{\mathrm{T}}\boldsymbol{S}_2\boldsymbol{e}_{2d} - \boldsymbol{z}_3^{\mathrm{T}}\boldsymbol{S}_3\boldsymbol{e}_{3d}. \tag{26}$$

Step 4. Design of actual control input $\boldsymbol{U}_1$.

We chose the following Lyapunov function:

$$V_4 = \frac{1}{2}\boldsymbol{z}_4^{\mathrm{T}}\boldsymbol{z}_4 + V_3. \tag{27}$$

From (22) and (26), the time derivative of V_4 is

$$\begin{aligned}\dot{V}_4 = &-k_1\boldsymbol{z}_1^{\mathrm{T}}\boldsymbol{z}_1 - k_2\boldsymbol{z}_2^{\mathrm{T}}\boldsymbol{z}_2 - k_3\boldsymbol{z}_3^{\mathrm{T}}\boldsymbol{z}_3 + \boldsymbol{z}_2^{\mathrm{T}}\tilde{\boldsymbol{D}}_1 + \boldsymbol{z}_3^{\mathrm{T}}\boldsymbol{S}_3\boldsymbol{z}_4\\ &-\boldsymbol{z}_2^{\mathrm{T}}\boldsymbol{S}_2\boldsymbol{e}_{2d} - \boldsymbol{z}_3^{\mathrm{T}}\boldsymbol{S}_3\boldsymbol{e}_{3d} + \boldsymbol{z}_4^{\mathrm{T}}(\boldsymbol{R}_4\boldsymbol{x}_4 + \boldsymbol{S}_4\boldsymbol{U}_1 + \boldsymbol{D}_2 - \dot{\alpha}_3).\end{aligned} \tag{28}$$

The following DOB is used to estimate disturbance $\boldsymbol{D}_2$ [46],

$$\begin{cases}\hat{\mathbf{D}}_2 = \boldsymbol{T}_2 + Q(\boldsymbol{x}_4),\\ \dot{\mathbf{T}}_2 = L(\boldsymbol{x}_4)\{-\boldsymbol{R}_4\boldsymbol{x}_4 - \boldsymbol{S}_4\boldsymbol{U}_1 - [\boldsymbol{T}_2 + Q(\boldsymbol{x}_4)]\},\end{cases} \tag{29}$$

where

$$Q(\boldsymbol{x}_4) = \begin{bmatrix}\mu_3(\dot{\theta}^{\varepsilon_3} + \dot{\theta}^{\varepsilon_3}/\varepsilon_3)\\ \mu_4(\dot{\phi}^{\varepsilon_4} + \dot{y}^{\varepsilon_4}/\varepsilon_4)\end{bmatrix}, \quad L(\boldsymbol{x}_4) = \frac{\partial Q(\boldsymbol{x}_4)}{\partial \boldsymbol{x}_4} = \begin{bmatrix}\mu_3(1+\dot{\theta}^{\varepsilon_3-1}) & 0\\ 0 & \mu_4(1+\dot{\phi}^{\varepsilon_4-1})\end{bmatrix}, \quad \mu_i > 0,$$

and ε_j $(i = 3, 4; j = 3, 4)$ is a positive odd constant.

Based on (28) and (29), the actual control input $\boldsymbol{U}_1$ is designed as

$$\boldsymbol{U}_1 = \boldsymbol{S}_4^{-1}(-\boldsymbol{R}_4\boldsymbol{x}_4 - k_4\boldsymbol{z}_4 + \dot{\alpha}_3 - \boldsymbol{z}_3^{\mathrm{T}}\boldsymbol{S}_3 - \hat{\boldsymbol{D}}_2). \tag{30}$$

Substituting (30) into (28), we obtain

$$\dot{V}_4 = -k_1\boldsymbol{z}_1^{\mathrm{T}}\boldsymbol{z}_1 - k_2\boldsymbol{z}_2^{\mathrm{T}}\boldsymbol{z}_2 - k_3\boldsymbol{z}_3^{\mathrm{T}}\boldsymbol{z}_3 - k_4\boldsymbol{z}_4^{\mathrm{T}}\boldsymbol{z}_4 + \boldsymbol{z}_2^{\mathrm{T}}\tilde{\boldsymbol{D}}_1 + \boldsymbol{z}_4^{\mathrm{T}}\tilde{\boldsymbol{D}}_2 - \boldsymbol{z}_2^{\mathrm{T}}\boldsymbol{S}_2\boldsymbol{e}_{2d} - \boldsymbol{z}_3^{\mathrm{T}}\boldsymbol{S}_3\boldsymbol{e}_{3d}. \tag{31}$$

Remark 1. Both the adaptive technique and the DOB can tackle the uncertainty of the nonlinear system. The adaptive method is used to estimate the bounds of the uncertainty, while the DOB estimates the uncertainty itself. Compared with the adaptive technique, the DOB makes the controller design more convenient and flexible. The DOB is applied as a compensator to effectively suppress unknown uncertainties and external disturbances. It does not rely on the system's mathematical model, and it can estimate the external disturbances of the controlled object in real time and actively compensate them for a limited period of time [39]. In view of the aforementioned good performance of the DOB, the DOB-based backstepping method is used to design the controller for subsystem Σ_1. Additionally, we can verify from our comparative simulation results between the adaptive backstepping control method and the designed DOB-based control scheme that the designed DOB-based control scheme yields a better performance than the adaptive backstepping control method.

3.2 Subsystem $\boldsymbol{\Sigma_2}$ controller design

In this subsection, a control scheme is designed for the fully actuated subsystem Σ_2 with disturbance $\boldsymbol{D}_3$ based on the combination of the SMC and DOB methods.

For nonlinear systems, a linear sliding mode surface is used to design a controller in many sliding mode control schemes. In order to alleviate the chattering problem and improve the convergence speed of the sliding mode surface, the nonlinear sliding mode surface for Σ_2 is designed as

$$\boldsymbol{s} = \dot{\boldsymbol{e}} + \int_0^{\sigma} l_0\mathrm{sgn}(\boldsymbol{e})\|\boldsymbol{e}\|^{\omega_0} + l_1\mathrm{sgn}(\dot{\boldsymbol{e}})\|\dot{\boldsymbol{e}}\|^{\omega_1}\mathrm{d}\sigma, \tag{32}$$

where $l_0 > 0$, $l_1 > 0$, $\omega_0, \omega_1 \in (0, 1)$, $\boldsymbol{e} = [e_1\ e_2]^{\mathrm{T}}$, $\|\boldsymbol{e}\|^{\omega_0} = [|e_1|^{\omega_0}\ |e_2|^{\omega_0}]^{\mathrm{T}}$, $\dot{\boldsymbol{e}} = [\dot{e}_1\ \dot{e}_2]^{\mathrm{T}}$, $\|\dot{\boldsymbol{e}}\|^{\omega_1} = [|\dot{e}_1|^{\omega_1}\ |\dot{e}_2|^{\omega_1}]^{\mathrm{T}}$,

$$\mathrm{sgn}(\boldsymbol{e}) = \begin{bmatrix}\mathrm{sgn}(e_1) & 0\\ 0 & \mathrm{sgn}(e_2)\end{bmatrix}, \quad \mathrm{sgn}(\dot{\boldsymbol{e}}) = \begin{bmatrix}\mathrm{sgn}(\dot{e}_1) & 0\\ 0 & \mathrm{sgn}(\dot{e}_2)\end{bmatrix},$$

and the tracking error of $\boldsymbol{x}_5$ is defined as

$$\boldsymbol{e} = \boldsymbol{x}_5 - \boldsymbol{x}_{5d}. \tag{33}$$

From (32) and (33) and Σ_2, the time derivative of $\boldsymbol{s}$ is

$$\dot{\mathbf{s}} = \boldsymbol{R}_6\boldsymbol{x}_6 + \boldsymbol{S}_6\boldsymbol{U}_2 + \boldsymbol{F}_6 + \boldsymbol{D}_3 - \ddot{\mathbf{x}}_{5d} + l_0\mathrm{sgn}(\boldsymbol{e})\|\boldsymbol{e}\|^{\omega_0} + l_1\mathrm{sgn}(\dot{\boldsymbol{e}})\|\dot{\boldsymbol{e}}\|^{\omega_1}, \tag{34}$$

where $0 < \omega_1 < 1, \omega_0 = \frac{\omega_1}{2-\omega_1}$.

The following DOB is employed to estimate disturbance $\boldsymbol{D}_3$ [46],

$$\begin{cases} \hat{\boldsymbol{D}}_3 = \boldsymbol{T}_3 + Q(\boldsymbol{x}_6), \\ \dot{\boldsymbol{T}}_3 = L(\boldsymbol{x}_6)\{-\boldsymbol{R}_6\boldsymbol{x}_6 - \boldsymbol{S}_6\boldsymbol{U}_2 - \boldsymbol{F}_6 - [\boldsymbol{T}_3 + Q(\boldsymbol{x}_6)]\}, \end{cases} \tag{35}$$

where

$$Q(\boldsymbol{x}_6) = \begin{bmatrix} \mu_5(\dot{z}^{\varepsilon_5} + \dot{z}^{\varepsilon_5}/\varepsilon_5) \\ \mu_6(\dot{\psi}^{\varepsilon_6} + \dot{\psi}^{\varepsilon_6}/\varepsilon_6) \end{bmatrix}, \quad L(\boldsymbol{x}_6) = \frac{\partial Q(\boldsymbol{x}_6)}{\partial \boldsymbol{x}_6} = \begin{bmatrix} \mu_5(1 + \dot{z}^{\varepsilon_5 - 1}) & 0 \\ 0 & \mu_6(1 + \dot{\psi}^{\varepsilon_6 - 1}) \end{bmatrix}, \quad \mu_i > 0,$$

and ε_j $(i = 5, 6; j = 5, 6)$ is a positive odd constant.

Compared with the fast signal power reaching law, the double power reaching law has better global fast convergence performance. Thus, we design the double power reaching law as follows:

$$\dot{\boldsymbol{s}} = -h_1\mathrm{sgn}(\boldsymbol{s})\|\boldsymbol{s}\|^{\alpha} - h_2\mathrm{sgn}(\boldsymbol{s})\|\boldsymbol{s}\|^{\beta} - h_3\boldsymbol{s}, \tag{36}$$

where $\alpha > 1, 0 < \beta < 1, h_1, h_2, h_3 > 0, \boldsymbol{s} = [s_1\, s_2]^{\mathrm{T}}$, and

$$\|\boldsymbol{s}\|^{\Lambda} = \left[|s_1|^{\Lambda}\ |s_2|^{\Lambda}\right]^{\mathrm{T}}, \quad (\Lambda = \alpha, \beta), \quad \mathrm{sgn}(\boldsymbol{s}) = \begin{bmatrix} \mathrm{sgn}(s_1) & 0 \\ 0 & \mathrm{sgn}(s_2) \end{bmatrix}.$$

From (34)–(36), the control input is designed as

$$\begin{aligned} \boldsymbol{U}_2 = -{\boldsymbol{S}_6}^{-1}[&\boldsymbol{R}_6\boldsymbol{x}_6 + \boldsymbol{F}_6 + \hat{\boldsymbol{D}}_3 - \ddot{\boldsymbol{x}}_{5d} + l_0\mathrm{sgn}(\boldsymbol{e})\|\boldsymbol{e}\|^{\omega_0} \\ &+ l_1\mathrm{sgn}(\dot{\boldsymbol{e}})\|\dot{\boldsymbol{e}}\|^{\omega_1} + h_1\mathrm{sgn}(\boldsymbol{s})\|\boldsymbol{s}\|^{\alpha} + h_2\mathrm{sgn}(\boldsymbol{s})\|\boldsymbol{s}\|^{\beta} + h_3\boldsymbol{s}]. \end{aligned} \tag{37}$$

By substituting (35) and (37) into (34), Eq. (34) becomes

$$\dot{\mathbf{s}} = -h_1\mathrm{sgn}(\boldsymbol{s})\|\boldsymbol{s}\|^{\alpha} - h_2\mathrm{sgn}(\boldsymbol{s})\|\boldsymbol{s}\|^{\beta} - h_3\boldsymbol{s} + \tilde{\boldsymbol{D}}_3. \tag{38}$$

Remark 2. Compared with the traditional reaching law, the double power reaching law has the features of solving the chattering problem, shorter convergence time, and faster convergence speed. In this paper, the multivariable double power reaching law is applied for the designing sliding mode controller, which can ensure that the system state reaches the sliding surface in a finite amount of time.

The advantages of the designed sliding mode surface shown in (32) can be summarized as follows.

Remark 3. Generally, the sign function in traditional sliding mode control causes the chattering problem. Compared with the conventional linear sliding surface, the adopted sliding mode surface uses an integral term and the sliding mode surface is continuous. Although Eq. (32) includes sign functions, the terms $\mathrm{sgn}(\boldsymbol{e})\|\boldsymbol{e}\|^{\omega_0}$ and $\mathrm{sgn}(\dot{\boldsymbol{e}})\|\dot{\boldsymbol{e}}\|^{\omega_1}$ are continuous functions. Based on the above characteristics, the adopted sliding mode surface shown in (32) can suppress the chattering problem effectively, accelerate the convergence rate, and enhance the anti-disturbance capability of the system.

4 Stability analysis

In this section, the stability of the system is analyzed based on Lyapunov theory. This section contains three parts. The first part contains a stability analysis of DOB, the second part contains a stability analysis of subsystem Σ_1, and the last part contains a stability analysis of subsystem Σ_2.

4.1 Stability analysis of DOB

According to Assumption 1, we have

$$\dot{\boldsymbol{D}}_1 \approx [0\ \ 0]^{\mathrm{T}}, \quad \dot{\tilde{\boldsymbol{D}}}_1 = \dot{\boldsymbol{D}}_1 - \dot{\hat{\boldsymbol{D}}}_1. \tag{39}$$

Then, from (15), the following equation holds:

$$\begin{aligned} \dot{\tilde{\boldsymbol{D}}}_1 &= -L(\boldsymbol{x}_2)\{-\boldsymbol{R}_2\boldsymbol{x}_2 - \boldsymbol{S}_2\boldsymbol{x}_3 - [\boldsymbol{T}_1 + Q(\boldsymbol{x}_2)]\} - \frac{\partial Q(\boldsymbol{x}_2)}{\partial \boldsymbol{x}_2}\dot{\boldsymbol{x}}_2 \\ &= -L(\boldsymbol{x}_2)\{-\boldsymbol{R}_2\boldsymbol{x}_2 - \boldsymbol{S}_2\boldsymbol{x}_3 - [\boldsymbol{T}_1 + Q(\boldsymbol{x}_2)]\} - L(\boldsymbol{x}_2)\{\boldsymbol{R}_2\boldsymbol{x}_2 + \boldsymbol{S}_2\boldsymbol{x}_3 + \boldsymbol{D}_1\} \\ &= L(\boldsymbol{x}_2)(\hat{\boldsymbol{D}}_1 - \boldsymbol{D}_1) = -L(\boldsymbol{x}_2)\tilde{\boldsymbol{D}}_1. \end{aligned} \tag{40}$$

Similarly, we can obtain

$$\dot{\tilde{\boldsymbol{D}}}_2 = -L(\boldsymbol{x}_4)\tilde{\boldsymbol{D}}_2, \quad \dot{\tilde{\boldsymbol{D}}}_3 = -L(\boldsymbol{x}_6)\tilde{\boldsymbol{D}}_3. \tag{41}$$

The following Lyapunov functions are chosen:

$$V_5 = \frac{1}{2}\tilde{\boldsymbol{D}}_1^{\mathrm{T}}\tilde{\boldsymbol{D}}_1, \quad V_6 = \frac{1}{2}\tilde{\boldsymbol{D}}_2^{\mathrm{T}}\tilde{\boldsymbol{D}}_2, \quad V_7 = \frac{1}{2}\tilde{\boldsymbol{D}}_3^{\mathrm{T}}\tilde{\boldsymbol{D}}_3. \tag{42}$$

Based on (39), (40), and (42), the time derivatives of V_5, V_6, V_7 are

$$\dot{V}_5 \ = \ -\tilde{\boldsymbol{D}}_1^{\mathrm{T}}L(\boldsymbol{x}_2)\tilde{\boldsymbol{D}}_1 < 0, \quad \dot{V}_6 = -\tilde{\boldsymbol{D}}_2^{\mathrm{T}}L(\boldsymbol{x}_4)\tilde{\boldsymbol{D}}_2 < 0, \quad \dot{V}_7 = -\tilde{\boldsymbol{D}}_3^{\mathrm{T}}L(\boldsymbol{x}_6)\tilde{\boldsymbol{D}}_3 < 0. \tag{43}$$

It can be seen that the estimate errors $\tilde{\boldsymbol{D}}_1, \tilde{\boldsymbol{D}}_2, \tilde{\boldsymbol{D}}_3$ satisfy the Lyapunov stability criteria and will converge to a small neighborhood around zero. According to (40), we can get

$$\tilde{\boldsymbol{D}}_1(t) = \mathrm{e}^{-L(\boldsymbol{x}_2)(t-t_0)}\tilde{\boldsymbol{D}}_1(0), \quad \tilde{\boldsymbol{D}}_2(t) = \mathrm{e}^{-L(\boldsymbol{x}_4)(t-t_0)}\tilde{\boldsymbol{D}}_2(0), \quad \tilde{\boldsymbol{D}}_3(t) = \mathrm{e}^{-L(\boldsymbol{x}_6)(t-t_0)}\tilde{\boldsymbol{D}}_3(0), \tag{44}$$

where $\tilde{\boldsymbol{D}}_j(0)$ is the initial value of $\tilde{\boldsymbol{D}}_j$ $(j = 1, 2, 3)$. The estimate error initially reaches its maximum value and then exponentially converges to zero by selecting appropriate values for parameters $\mu_i, \varepsilon_i, i = 1, 2, 3, 4, 5, 6$.

4.2 Stability analysis of subsystem $\boldsymbol{\Sigma_1}$

In the presence of external disturbances, Lyapunov theory proves that the system is asymptotically stable with the designed controller and DOB.

From (17), (18), (24), and (25), we have

$$\dot{\alpha}_{2d} = \frac{-\boldsymbol{e}_{2d}}{\tau_1}, \quad \dot{\alpha}_{3d} = \frac{-\boldsymbol{e}_{3d}}{\tau_2}. \tag{45}$$

The filter estimate error dynamics are

$$\dot{\boldsymbol{e}}_{2d} = \frac{-\boldsymbol{e}_{2d}}{\tau_1} - \dot{\alpha}_2, \quad \dot{\boldsymbol{e}}_{3d} = \frac{-\boldsymbol{e}_{3d}}{\tau_2} - \dot{\alpha}_3. \tag{46}$$

We chose the following Lyapunov function:

$$V_8 = V_4 + V_5 + V_6 + \frac{1}{2}\boldsymbol{e}_{2d}^{\mathrm{T}}\boldsymbol{e}_{2d} + \frac{1}{2}\boldsymbol{e}_{3d}^{\mathrm{T}}\boldsymbol{e}_{3d}, \tag{47}$$

and based on (31) and (43), the time derivative of V_8 is

$$\begin{aligned} \dot{V}_8 &= -k_1\boldsymbol{z}_1^{\mathrm{T}}\boldsymbol{z}_1 - k_2\boldsymbol{z}_2^{\mathrm{T}}\boldsymbol{z}_2 - k_3\boldsymbol{z}_3^{\mathrm{T}}\boldsymbol{z}_3 - k_4\boldsymbol{z}_4^{\mathrm{T}}\boldsymbol{z}_4 + \boldsymbol{z}_2^{\mathrm{T}}\tilde{\boldsymbol{D}}_1 + \boldsymbol{z}_4^{\mathrm{T}}\tilde{\boldsymbol{D}}_2 - \tilde{\boldsymbol{D}}_1^{\mathrm{T}}L(\boldsymbol{x}_2)\tilde{\boldsymbol{D}}_1 - \tilde{\boldsymbol{D}}_2^{\mathrm{T}}L(\boldsymbol{x}_4)\tilde{\boldsymbol{D}}_2 \\ &\quad -\boldsymbol{z}_2^{\mathrm{T}}\boldsymbol{S}_2\boldsymbol{e}_{2d} - \boldsymbol{z}_3^{\mathrm{T}}\boldsymbol{S}_3\boldsymbol{e}_{3d} + \boldsymbol{e}_{2d}^{\mathrm{T}}\dot{\boldsymbol{e}}_{2d} + \boldsymbol{e}_{3d}^{\mathrm{T}}\dot{\boldsymbol{e}}_{3d} \\ &\leqslant -k_1\boldsymbol{z}_1^{\mathrm{T}}\boldsymbol{z}_1 - k_2\boldsymbol{z}_2^{\mathrm{T}}\boldsymbol{z}_2 - k_3\boldsymbol{z}_3^{\mathrm{T}}\boldsymbol{z}_3 - k_4\boldsymbol{z}_4^{\mathrm{T}}\boldsymbol{z}_4 + \frac{1}{2}\boldsymbol{z}_2^{\mathrm{T}}\boldsymbol{z}_2 + \frac{1}{2}\tilde{\boldsymbol{D}}_1^{\mathrm{T}}\tilde{\boldsymbol{D}}_1 + \frac{1}{2}\boldsymbol{z}_4^{\mathrm{T}}\boldsymbol{z}_4 + \frac{1}{2}\tilde{\boldsymbol{D}}_2^{\mathrm{T}}\tilde{\boldsymbol{D}}_2 \\ &\quad -\tilde{\boldsymbol{D}}_1^{\mathrm{T}}L(\boldsymbol{x}_2)\tilde{\boldsymbol{D}}_1 - \tilde{\boldsymbol{D}}_2^{\mathrm{T}}L(\boldsymbol{x}_4)\tilde{\boldsymbol{D}}_2 - \boldsymbol{z}_2^{\mathrm{T}}\boldsymbol{S}_2\boldsymbol{e}_{2d} - \boldsymbol{z}_3^{\mathrm{T}}\boldsymbol{S}_3\boldsymbol{e}_{3d} + \boldsymbol{e}_{2d}^{\mathrm{T}}\dot{\boldsymbol{e}}_{2d} + \boldsymbol{e}_{3d}^{\mathrm{T}}\dot{\boldsymbol{e}}_{3d} \\ &= -k_1\boldsymbol{z}_1^{\mathrm{T}}\boldsymbol{z}_1 - \left(k_2 - \frac{1}{2}\right)\boldsymbol{z}_2^{\mathrm{T}}\boldsymbol{z}_2 - k_3\boldsymbol{z}_3^{\mathrm{T}}\boldsymbol{z}_3 - \left(k_4 - \frac{1}{2}\right)\boldsymbol{z}_4^{\mathrm{T}}\boldsymbol{z}_4 - \tilde{\boldsymbol{D}}_1^{\mathrm{T}}\left[L(\boldsymbol{x}_2) - \frac{1}{2}\boldsymbol{E}\right]\tilde{\boldsymbol{D}}_1 \\ &\quad -\tilde{\boldsymbol{D}}_2^{\mathrm{T}}\left[L(\boldsymbol{x}_4) - \frac{1}{2}\boldsymbol{E}\right]\tilde{\boldsymbol{D}}_2 - \boldsymbol{z}_2^{\mathrm{T}}\boldsymbol{S}_2\boldsymbol{e}_{2d} - \boldsymbol{z}_3^{\mathrm{T}}\boldsymbol{S}_3\boldsymbol{e}_{3d} + \boldsymbol{e}_{2d}^{\mathrm{T}}\dot{\boldsymbol{e}}_{2d} + \boldsymbol{e}_{3d}^{\mathrm{T}}\dot{\boldsymbol{e}}_{3d}. \end{aligned} \tag{48}$$

Following the results found in [47,48], assume that Eqs. (16) and (23) satisfy $\|\dot{\alpha}_{2d}\| \leqslant r_{2d}$ and $\|\dot{\alpha}_{3d}\| \leqslant r_{3d}$, respectively. Then, based on (45) and (46), the last four terms of (48) satisfy

$$\begin{aligned}
&-(\boldsymbol{z}_2^{\mathrm{T}}\boldsymbol{S}_2\boldsymbol{e}_{2d}+\boldsymbol{z}_3^{\mathrm{T}}\boldsymbol{S}_3\boldsymbol{e}_{3d})+\boldsymbol{e}_{2d}^{\mathrm{T}}\dot{\boldsymbol{e}}_{2d}+\boldsymbol{e}_{3d}^{\mathrm{T}}\dot{\boldsymbol{e}}_{3d}\\
&\leqslant \frac{1}{2a_4^2}\|\boldsymbol{S}_2\|^2\|\boldsymbol{z}_2^{\mathrm{T}}\|^2+\frac{a_4^2\|\boldsymbol{e}_{2d}\|^2}{2}+\frac{1}{2a_5^2}\|\boldsymbol{S}_3\|^2\|\boldsymbol{z}_3^{\mathrm{T}}\|^2+\frac{a_5^2\|\boldsymbol{e}_{3d}\|^2}{2}\\
&\quad+\boldsymbol{e}_{2d}^{\mathrm{T}}\left(\frac{-\boldsymbol{e}_{2d}}{\tau_1}-\dot{\alpha}_2\right)+\boldsymbol{e}_{3d}^{\mathrm{T}}\left(\frac{-\boldsymbol{e}_{3d}}{\tau_2}-\dot{\alpha}_3\right)\\
&\leqslant \frac{1}{2a_4^2}\|\boldsymbol{S}_2\|^2\|\boldsymbol{z}_2^{\mathrm{T}}\|^2+\frac{a_4^2\|\boldsymbol{e}_{2d}\|^2}{2}+\frac{1}{2a_5^2}\|\boldsymbol{S}_3\|^2\|\boldsymbol{z}_3^{\mathrm{T}}\|^2+\frac{a_5^2\|\boldsymbol{e}_{3d}\|^2}{2}-\frac{\|\boldsymbol{e}_{2d}\|^2}{\tau_1}-\frac{\|\boldsymbol{e}_{3d}\|^2}{\tau_2}\\
&\quad+\frac{a_2^2}{2}\|\boldsymbol{e}_{2d}\|^2 r_{2d}+\frac{1}{2a_2^2}+\frac{a_3^2}{2}\|\boldsymbol{e}_{3d}\|^2 r_{3d}+\frac{1}{2a_3^2}.
\end{aligned} \tag{49}$$

After replacing (49) into (48), the latter one yields

$$\begin{aligned}
\dot{V}_8 \leqslant& -k_1\boldsymbol{z}_1^{\mathrm{T}}\boldsymbol{z}_1-\left(k_2-\frac{1}{2}-\frac{1}{2a_4^2}\|\boldsymbol{S}_2\|^2\right)\boldsymbol{z}_2^{\mathrm{T}}\boldsymbol{z}_2-\left(k_3-\frac{1}{2a_5^2}\|\boldsymbol{S}_3\|^2\right)\boldsymbol{z}_3^{\mathrm{T}}\boldsymbol{z}_3-\left(k_4-\frac{1}{2}\right)\boldsymbol{z}_4^{\mathrm{T}}\boldsymbol{z}_4\\
&-\tilde{\boldsymbol{D}}_1^{\mathrm{T}}\left[L(\boldsymbol{x}_2)-\frac{1}{2}\boldsymbol{E}\right]\tilde{\boldsymbol{D}}_1-\tilde{\boldsymbol{D}}_2^{\mathrm{T}}\left[L(\boldsymbol{x}_4)-\frac{1}{2}\boldsymbol{E}\right]\tilde{\boldsymbol{D}}_2-\left(\frac{1}{\tau_1}-\frac{a_4^2}{2}-\frac{a_2^2}{2}r_{2d}\right)\|\boldsymbol{e}_{2d}\|^2\\
&-\left(\frac{1}{\tau_2}-\frac{a_5^2}{2}-\frac{a_3^2}{2}r_{3d}\right)\|\boldsymbol{e}_{3d}\|^2+\frac{1}{2a_2^2}+\frac{1}{2a_3^2}\\
\leqslant& -2\kappa V_8+C,
\end{aligned} \tag{50}$$

where $a_2,a_3,a_4,a_5>0, k_2>\frac{1}{2}+\frac{1}{2a_4^2}\|\boldsymbol{S}_2\|^2, k_3>\frac{1}{2a_5^2}\|\boldsymbol{S}_3\|^2, k_4>\frac{1}{2}, 0<\tau_1<\frac{2}{a_4^2+a_2^2r_{2d}}, 0<\tau_2<\frac{2}{a_5^2+a_3^2r_{3d}}$, $C=\frac{1}{2a_2^2}+\frac{1}{2a_3^2}, \kappa=\min\{k_1,k_2-\frac{1}{2}-\frac{1}{2a_4^2}\|\boldsymbol{S}_2\|^2,k_3-\frac{1}{2a_5^2}\|\boldsymbol{S}_3\|^2,k_4-\frac{1}{2},\frac{1}{\tau_1}-\frac{a_4^2}{2}-\frac{a_2^2}{2}r_{2d},\frac{1}{\tau_2}-\frac{a_5^2}{2}-\frac{a_3^2}{2}r_{3d}\}$, $L(\boldsymbol{x}_2),L(\boldsymbol{x}_4)>\frac{1}{2}\boldsymbol{E}$ (the elements of $L(\boldsymbol{x}_2),L(\boldsymbol{x}_4)$ are larger than those of $\frac{1}{2}\boldsymbol{E}, \boldsymbol{E}$ is a diagonal matrix).

From (50), it can be seen that when $V_8=\varsigma, \dot{V}_8\leqslant-2\kappa\varsigma+C$; if $\kappa\geqslant 2c\varsigma, c>0$, then $\dot{V}_8\leqslant 0$ on $V_8=\varsigma$, and so $V_8\leqslant\varsigma$ is an invariant set, i.e., if $V_8(0)\leqslant\varsigma$, then $V_8(t)\leqslant\varsigma$ for all $t\geqslant 0$. Therefore, Eq. (50) holds for all $V_8(t)\leqslant\varsigma$ and $t\geqslant 0$.

Standard arguments can now be applied to solve (50) as follows:

$$0\leqslant V_8(t)\leqslant\frac{C}{2\kappa}+\left(V_8(0)-\frac{C}{2\kappa}\right)\exp(-2\kappa t),\quad \forall t\geqslant 0. \tag{51}$$

It is clear that $V_8(t)$ is bounded by $\frac{C}{2\kappa}$, i.e., for $t\geqslant 0$, $0\leqslant V_8(t)\leqslant\frac{C}{2\kappa}$.

From (51), the tracking error of $\boldsymbol{x}_1$ yields

$$\|\boldsymbol{z}_1\|\leqslant\sqrt{\frac{C}{\kappa}+\left(2V_8(0)-\frac{C}{\kappa}\right)\exp(-2\kappa t)}. \tag{52}$$

Thus, we can obtain the following inequality: $\|\boldsymbol{z}_1\|\leqslant\sqrt{\frac{C}{\kappa}}$.

Then, the convergence region of $\boldsymbol{z}_1$ can be expressed as

$$R=\left\{\boldsymbol{z}_1\left|\|\boldsymbol{z}_1\|\leqslant\sqrt{\frac{C}{\kappa}}\right.\right\}. \tag{53}$$

From (53), the tracking error can be made to converge to an arbitrarily small region around zero by making κ sufficiently large, which can be achieved by properly selecting the design parameters in (54).

4.3 Stability analysis of subsystem Σ_2

For subsystem Σ_2, to analyze the reachability of the sliding states, the following Lyapunov function is chosen:

$$V_9 = \frac{1}{2}\boldsymbol{s}^{\mathrm{T}}\boldsymbol{s} + \frac{1}{2}\tilde{\boldsymbol{D}}_3^{\mathrm{T}}\tilde{\boldsymbol{D}}_3. \tag{54}$$

Its time derivative satisfies

$$\begin{aligned}\dot{V}_9 &= -h_1\|\boldsymbol{s}\|^{\alpha+1} - h_2\|\boldsymbol{s}\|^{\beta+1} - h_3\|\boldsymbol{s}\|^2 + \boldsymbol{s}^{\mathrm{T}}\tilde{\boldsymbol{D}}_3 - \tilde{\boldsymbol{D}}_3^{\mathrm{T}}L(\boldsymbol{x}_6)\tilde{\boldsymbol{D}}_3\\ &\leqslant -h_1\|\boldsymbol{s}\|^{\alpha+1} - h_2\|\boldsymbol{s}\|^{\beta+1} - (h_3 - \tfrac{1}{2})\|\boldsymbol{s}\|^2 - \tilde{\boldsymbol{D}}_3^{\mathrm{T}}(L(\boldsymbol{x}_6) - \tfrac{1}{2}\boldsymbol{E})\tilde{\boldsymbol{D}}_3.\end{aligned} \tag{55}$$

As long as $h_3 > \frac{1}{2}, L(\boldsymbol{x}_6) > \frac{1}{2}\boldsymbol{E}$ (as long as the elements of $L(\boldsymbol{x}_6)$ are larger than those of $\frac{1}{2}\boldsymbol{E}, \boldsymbol{E}$ is a diagonal matrix), $\dot{V}_9 \leqslant 0$. From (55), we can determine that the sliding states can reach the sliding surface exponentially, i.e., $\boldsymbol{s} = \boldsymbol{0}$. Based on the reachability of the sliding surface, the stability analysis of the tracking error is done as follows.

The following Lyapunov function is chosen:

$$V_{10} = \frac{1}{2}\boldsymbol{e}^{\mathrm{T}}\boldsymbol{e}. \tag{56}$$

From (56) and because $\boldsymbol{e} = [e_1\ e_2]^{\mathrm{T}}, \dot{\boldsymbol{e}} = [\dot{e}_1\ \dot{e}_2]^{\mathrm{T}}$, the time derivative of V_{10} is

$$\dot{V}_{10} = \boldsymbol{e}^{\mathrm{T}}\dot{\boldsymbol{e}} = e_1\dot{e}_1 + e_2\dot{e}_2. \tag{57}$$

Based on $\boldsymbol{s} = \boldsymbol{0}$ and (32), $\dot{\boldsymbol{e}} = -\int_0^{\sigma} l_0\mathrm{sgn}(\boldsymbol{e})\|\boldsymbol{e}\|^{\omega_0} + l_1\mathrm{sgn}(\dot{\boldsymbol{e}})\|\dot{\boldsymbol{e}}\|^{\omega_1}\mathrm{d}\sigma$, i.e.,

$$\dot{e}_1 = -\int_0^{\sigma} l_0\mathrm{sgn}(e_1)|e_1|^{\omega_0} + l_1\mathrm{sgn}(\dot{e}_1)|\dot{e}_1|^{\omega_1}\mathrm{d}\sigma, \quad \dot{e}_2 = -\int_0^{\sigma} l_0\mathrm{sgn}(e_2)|e_2|^{\omega_0} + l_1\mathrm{sgn}(\dot{e}_2)|\dot{e}_2|^{\omega_1}\mathrm{d}\sigma. \tag{58}$$

To proceed, we prove that $e_1, \dot{e}_1$ have different signals, i.e., $e_1\dot{e}_1 < 0$. Here, we only prove that $e_1\dot{e}_1 < 0$, and $e_2\dot{e}_2 < 0$ can be obtained using the same method. We carry out a proof by contradiction. (a) Assume that $e_1, \dot{e}_1 > 0$. From (32), $\dot{e}_1 = -\int_0^{\sigma} l_0|e_1|^{\omega_0} + l_1|\dot{e}_1|^{\omega_1}\mathrm{d}\sigma < 0$, which contradicts $\dot{e}_1 > 0$. (b) Assume that $e_1, \dot{e}_1 < 0$. From (32) $\dot{e}_1 = \int_0^{\sigma} l_0|e_1|^{\omega_0} + l_1|\dot{e}_1|^{\omega_1}\mathrm{d}\sigma > 0$, which contradicts $\dot{e}_1 < 0$.

Based on the above analysis, we can obtain that $e_1\dot{e}_1 < 0$, and, by the same token, $e_2\dot{e}_2 < 0$. Thus, we can determine that $\dot{V}_{10} < 0$, that is to say, the tracking error is asymptotically stable. In conclusion, the tracking error is asymptotically stable, and the actual position of the QUAV (x, y, z) can reach the desired position, x_d, y_d, z_d.

5 Simulation and analysis

In this section, the effectiveness of the proposed control scheme is validated, and our simulations carried out using Matlab R2010a/Simulink are presented. Moreover, a comparative simulation between the designed control approach and the ABC approach is presented.

The reference commands are chosen as $x_d(t) = \sin(\frac{2\pi}{50}t), y_d(t) = \cos(\frac{2\pi}{50}t), z_d(t) = \frac{1}{6}t$, and the initial flight conditions of the QUAV are $x(0) = 0.07, y(0) = 1, z(0) = 0, \phi(0) = 0, \theta(0) = 0, \psi(0) = 0$. Additionally, the external disturbances are $\boldsymbol{D}_1 = [2\sin(t)\ 2\sin(t)]^{\mathrm{T}}, \boldsymbol{D}_2 = [0.2\sin(\frac{2\pi}{25}t)\ 0.2\sin(\frac{2\pi}{25}t)]^{\mathrm{T}}$, $\boldsymbol{D}_3 = [0.2\sin(\frac{2\pi}{25}t)\ \ 0.2\sin(\frac{2\pi}{25}t)]^{\mathrm{T}}$. The parameters of the QUAV model are given in Table 1, and the controller parameters are listed in Table 2. The efficiency of the designed control scheme (DOBC) in Section 3 is verified by comparing it with the ABC approach.

The control inputs $\boldsymbol{U}_1, \boldsymbol{U}_2$ under the ABC approach are designed as

$$\begin{aligned}\boldsymbol{U}_1 &= -\boldsymbol{S}_4^{-1}\left(\boldsymbol{R}_4\boldsymbol{x}_4 + k_4\boldsymbol{z}_4 + \boldsymbol{z}_3^{\mathrm{T}}\boldsymbol{S}_3 + \frac{\hat{p}_4 b_4\boldsymbol{z}_4}{\|\boldsymbol{z}_4\| + \xi_4}\right),\\ \boldsymbol{U}_2 &= -\boldsymbol{S}_6{}^{-1}\left(\boldsymbol{R}_6\boldsymbol{x}_6 + \boldsymbol{F}_6 + \boldsymbol{z}_5 + k_6\boldsymbol{z}_6 + \frac{\hat{p}_6 b_6\boldsymbol{z}_6}{\|\boldsymbol{z}_6\| + \xi_6}\right)\end{aligned} \tag{59}$$

Table 1 Quadrotor model parameters

Variable	Value	Unit	Variable	Value	Unit
m	2	kg	J_{yy}	1.25	$\mathrm{kg \cdot m^2}$
g	9.81	$\mathrm{m/s^2}$	J_{zz}	2.5	$\mathrm{kg \cdot m^2}$
a	0.2	m	$K_1 \sim K_3$	0.01	kg/s
J_{xx}	1.25	$\mathrm{kg \cdot m^2}$	$K_4 \sim K_6$	0.012	kg/s

Table 2 Controller parameters under DOBC

Variable	Value	Variable	Value	Variable	Value	Variable	Value
k_1	3.6	β	0.9	ω_0	2/3	ε_1	40
k_2	1	$l_0 \sim l_1$	0.5	ω_1	0.8	ε_2	5
k_3	50	h_1	0.01	τ_1	0.999	ε_3	50
k_4	1	h_2	0.015	τ_2	0.02	ε_4	0.00001
α	2	h_3	1	$\mu_1 \sim \mu_6$	1	$\varepsilon_5 \sim \varepsilon_6$	0.0000005

Table 3 Controller parameters under the ABC approach

Variable	Value	Variable	Value	Variable	Value	Variable	Value
k_1	0.5	k_5, k_6	0.005	b_1	2	ξ_2	5
k_2	0.5	v_1	0.5	b_2	500	ξ_3	5
k_3	80	v_2	0.5	b_3	50	τ_1	0.999
k_4	0.000005	v_3	0.5	ξ_1	5	τ_2	0.008

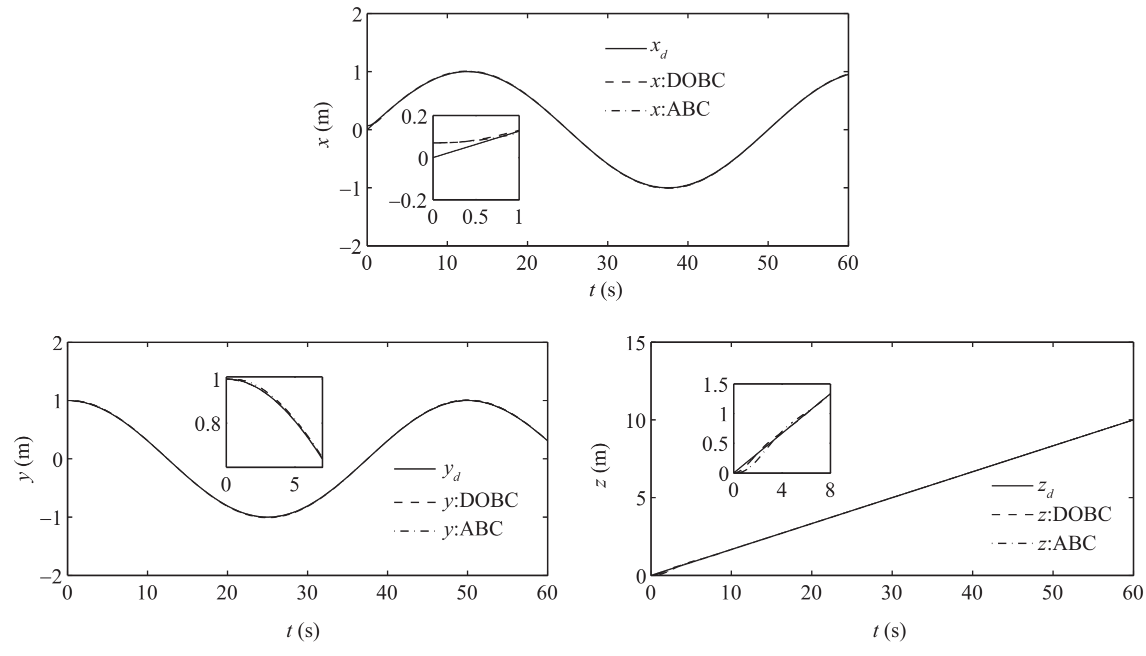

Figure 2 Time responses of position tracking under DOBC and ABC.

with the following adaptive law:

$$\dot{\hat{p}}_j = \begin{cases} v_j b_j \|\boldsymbol{z}_j\|^2/(\|\boldsymbol{z}_j\| + \xi_j), & \|\boldsymbol{z}_j\| > \xi_j/(b_j - 1), \\ 0, & \|\boldsymbol{z}_j\| \leqslant \xi_j/(b_j - 1), \end{cases} \tag{60}$$

where v_j, b_j, ξ_j $(j = 2, 4, 6), k_6$ are positive constants and $\xi_j > 1$. From (60), it can be seen that after the errors $\boldsymbol{z}_2, \boldsymbol{z}_4, \boldsymbol{z}_6$ become stable, the estimate rate stays at zero, which means that $\hat{p}$ does not change, thus avoiding the problem of overestimation.

The controller parameters under the ABC approach are listed in Table 3. The comparative simulation results for DOBC and ABC are shown in Figure 2 through 6. The local time response is also given to

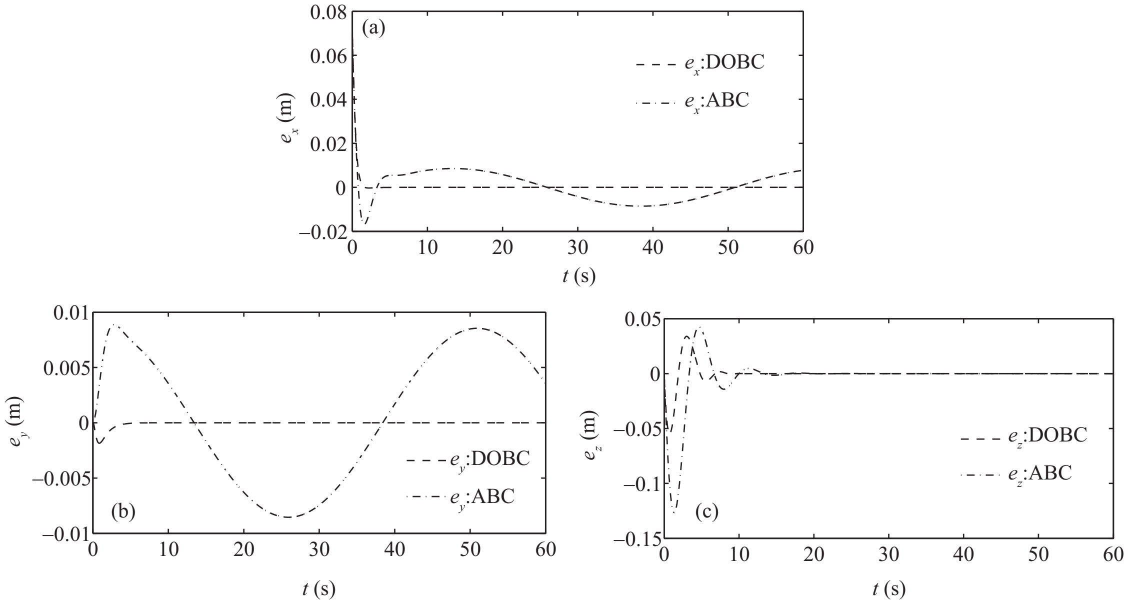

Figure 3 Time responses of the tracking errors under DOBC and ABC.

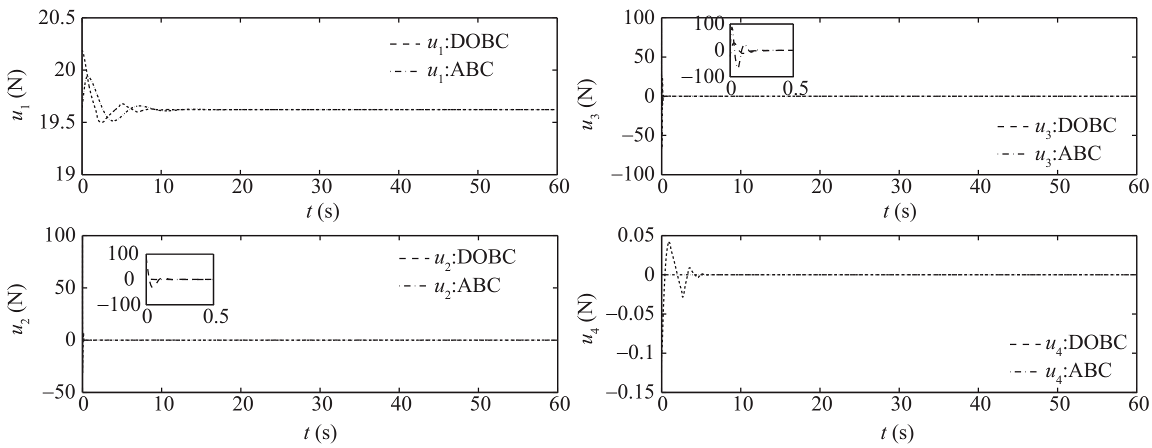

Figure 4 Time responses of the control inputs under DOBC and ABC.

better show the dynamic processes.

Figures 2 and 3 present the tracking performance of the QUAV under the two control methods. As can be seen from Figure 2, stable tracking of the position in the x, y, z directions of their respective reference commands was achieved after a short time. Figure 3 describes the trajectory tracking error curve of the system under the two control methods. We can observe that the two methods have different tracking performances. In detail, the tracking errors e_x, e_y become stable under the DOBC approach within 4 s, the tracking error e_x ranges from 0 to 0.08 m, and e_y ranges from -0.003 to 0 m. Besides, the tracking error e_z reaches stability within 10 s under the DOBC approach, and ranges from -0.06 to 0.04 m. In contrast, the tracking errors e_x, e_y under the ABC approach cannot achieve stability within 50 s. The tracking error e_y ranges from -0.01 to 0.01 m, which is larger than that of DOBC approach. Although the tracking error e_z under the ABC approach tends to be stable at approximately 15 s, its range of variation is large.

The time response of the control inputs under the two control schemes are provided in Figure 4; it can be seen that the control inputs of the DOBC approach are smooth. The time responses of ϕ, θ, ψ under the two control schemes are shown in Figure 5. We can see in Figure 5 that they are all stable. It can be seen from Figure 6 that the designed control scheme can make the sliding states reach the sliding surface

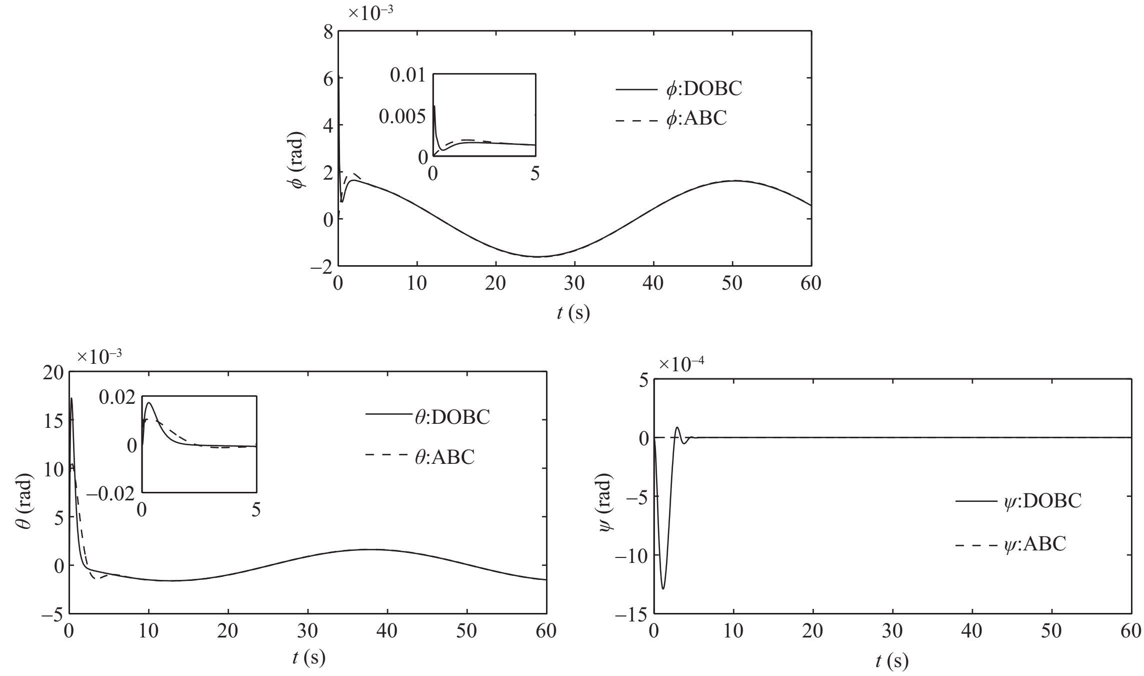

Figure 5 Time responses of ϕ, θ, ψ.

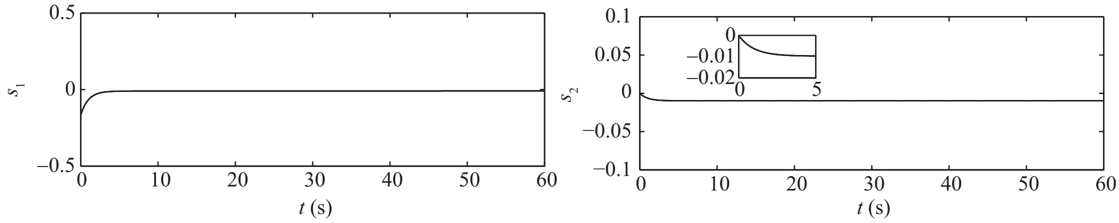

Figure 6 Time responses of sliding mode surface $\boldsymbol{s}$.

in less than five seconds.

With respect to the ABC approach, the simulation results given in Figure 2 through 6 under the proposed control scheme show better performances, higher precision tracking, faster convergence, and robustness.

6 Conclusion

In this paper, a DOB-based backstepping sliding mode controller was proposed to solve the trajectory tracking problem of QUAVs. First, the dynamic model of a QUAV was decomposed into two subsystems. Then, the DOB was proposed to estimate the external disturbances, and the DOB-based backstepping controller was designed for the first subsystem. To proceed, the SMC method based on DOB was employed to design the controller for the second subsystem. Then, the tracking error was proved to be asymptotically stable. Finally, by comparing the simulation results of a system under the designed control scheme and the ABC method, we found that the proposed control scheme achieved better and more stable tracking of the QUAV's position. Our future work will focus on position and attitude tracking controller design for QUAVs, while taking into consideration external disturbance, parametric uncertainties, and input constraints.

Acknowledgements This work was supported in part by National Natural Science Foundation of China (Grant Nos. 61503323, 61673294), Natural Science Foundation of Hebei Province (Grant Nos. F2017203130, A2016203341), the Foundation of Hebei Province Education Department (Grant No. QN2016076), and Postdoctoral Science Foundation of China (Grant No. 2015M571282). The authors would like to thank the editor and all anonymous reviewers for their comments, which helped to improve the quality of this paper.

References

1 Siebert S, Teizer J. Mobile 3D mapping for surveying earthwork projects using an unmanned aerial vehicle (UAV) system. Automat Constr, 2014, 41: 1–14
2 García-Delgado L G, Dzul A, Santibáñez V, et al. Quad-rotors formation based on potential functions with obstacle avoidance. IET Control Theor Appl, 2012, 6: 1787–1802
3 Wang K L, Ke Y J, Chen B M. Autonomous reconfigurable hybrid tail-sitter UAV U-Lion. Sci China Inf Sci, 2017, 60: 033201
4 Kacimi A, Mokhtari A, Kouadri B. Sliding mode control based on adaptive backstepping approach for a quadrotor unmanned aerial vehicle. Prz Elektrotechniczn, 2012, 88: 188–193
5 Tayebi A, McGilvray S. Attitude stabilization of a VTOL quadrotor aircraft. IEEE Trans Contr Syst Technol, 2006, 14: 562–571
6 Rodriguez R H, Vega P V, Orta S A, et al. Robust backstepping control based on integral sliding modes for tracking of quadrotors. J Intell Robot Syst, 2014, 73: 51–66
7 Liu X C, Wang H, Fu D, et al. An area-based position and attitude estimation for unmanned aerial vehicle navigation. Sci China Technol Sci, 2015, 58: 916–926
8 Peng K M, Lin F, Chen B M. Online schedule for autonomy of multiple unmanned aerial vehicles. Sci China Inf Sci, 2017, 60: 072203
9 Seyedtabaii S. New flat phase margin fractional order PID design: perturbed UAV roll control study. Robot Auton Syst, 2017, 96: 58–64
10 Rubio J J, Gomez J C, Cortes C A, et al. Experimental control of a fuel cell. IEEE Latin Am Trans, 2015, 13: 2935–2940
11 Drouot A, Zasadzinski M, Souley A H, et al. Two robust static output feedback control architectures for a gun launched micro aerial vehicle. In: Proceedings of the 21st Mediterranean Conference on Control and Automation (MED), Platanias-Chania, 2013. 25–28
12 Pounds P E, Bersak D R, Dollar A M. Stability of small-scale UAV helicopters and quadrotors with added payload mass under PID control. Auton Robot, 2012, 33: 129–142
13 Dinh T X, Nam D N C, Ahn K K. Robust attitude control and virtual reality model for quadrotor. Int J Autom Technol, 2015, 9: 283–290
14 Choi I H, Bang H C. Adaptive command filtered backstepping tracking controller design for quadrotor unmanned aerial vehicle. Proc Institution Mech Eng Part G-J Aerospace Eng, 2012, 226: 483–497
15 Li P, Yu X, Peng X Y, et al. Fault-tolerant cooperative control for multiple UAVs based on sliding mode techniques. Sci China Inf Sci, 2017, 60: 070204
16 Madani T, Benallegue A. Sliding mode observer and backstepping control for a quadrotor unmanned aerial vehicles. In: Proceedings of American Control Conference, 2007. 5887–5892
17 Zuo Z. Trajectory tracking control design with command-filtered compensation for a quadrotor. IET Control Theor Appl, 2010, 4: 2343–2355
18 He T P, Liu H, Li S. Quaternion-based robust trajectory tracking control for uncertain quadrotors. Sci China Inf Sci, 2016, 59: 122902
19 Wang Y, Wang D B. Tight formation control of multiple unmanned aerial vehicles through an adaptive control method. Sci China Inf Sci, 2017, 60: 070207
20 Zhang X B, Zhang Y M. Fault tolerant control for quad-rotor UAV by employing Lyapunov-based adaptive control approach. In: Proceedings of AIAA Guidance, Navigation, and Control Conference, 2010
21 Khebbache H, Sait B, Bounar N, et al. Robust stabilization of a quad-rotor UAV in presence of actuator and sensor faults. Int J Instrum Control Syst, 2012, 2: 53–67
22 Zheng Z, Xia Y Q, Fu M Y. Attitude stabilization of rigid spacecraft with finite-time convergence. Int J Robust Nonlin Control, 2011, 21: 686–702
23 Gao Y B, Luo W S, Liu J X, et al. Integral sliding mode control design for nonlinear stochastic systems under imperfect quantization. Sci China Inf Sci, 2017, 60: 120206
24 Yu W W, Wang H, Hong H F, et al. Distributed cooperative anti-disturbance control of multi-agent systems: an overview. Sci China Inf Sci, 2017, 60: 110202
25 Tian B L, Yin L P, Wang H. Finite-time reentry attitude control based on adaptive multivariable disturbance compensation. IEEE Trans Ind Electron, 2015, 62: 5889–5898
26 Tian B L, Liu L H, Lu H C, et al. Multivariable finite time attitude control for quadrotor UAV: theory and experimentation. IEEE Trans Ind Electron, 2018, 65: 2567–2577
27 Tian B L, Lu H C, Zuo Z Y, et al. Multivariable finite-time output feedback trajectory tracking control of quadrotor helicopters. Int J Robust Nonlin Control, 2018, 28: 281–295
28 Fang X, Wu A G, Shang Y J, et al. Multivariable super twisting based robust trajectory tracking control for small unmanned helicopter. Math Problems Eng, 2015, 10: 1–13

29 Fang X, Wu A G, Shang Y J, et al. A novel sliding mode controller for small-scale unmanned helicopters with mismatched disturbance. Nonlin Dyn, 2016, 83: 1053–1068
30 Mofid O, Mobayen S. Adaptive sliding mode control for finite-time stability of quad-rotor UAVs with parametric uncertainties. ISA Trans, 2017, 72: 1–14
31 Xu R, Ozguner U. Sliding mode control of a quadrotor helicopter. In: Proceedings of the 45th IEEE Conference on Decision and Control, San Diego, 2006. 4957–4962
32 Tian B L, Fan W R, Su R, et al. Real-time trajectory and attitude coordination control for reusable launch vehicle in reentry phase. IEEE Trans Ind Electron, 2015, 62: 1639–1650
33 Tian B L, Fan W R, Zong Q. Integrated guidance and control for reusable launch vehicle in reentry phase. Nonlin Dyn, 2015, 80: 397–412
34 Dierks T, Jagannathan S. Output feedback control of a quadrotor UAV using neural networks. IEEE Trans Neural Netw, 2010, 21: 50–66
35 Wang F, Hua C C, Zong Q. Attitude control of reusable launch vehicle in reentry phase with input constraint via robust adaptive backstepping control. Int J Adapt Control Signal Process, 2015, 29: 1308–1327
36 Wang F, Zou Q, Zong Q. Robust adaptive backstepping control for an uncertain nonlinear system with input constraint based on Lyapunov redesign. Int J Control Autom Syst, 2017, 15: 212–225
37 Cao L J, Hu X X, Zhang S X, et al. Robust flight control design using sensor-based backstepping control for unmanned aerial vehicles. J Aerosp Eng, 2017, 30: 04017068
38 Lee D J. Distributed backstepping control of multiple thrust-propelled vehicles on a balanced graph. Automatica, 2012, 48: 2971–2977
39 Tinashe C, Otis N. Adaptive sliding backstepping control of quadrotor UAV attitude. IFAC Proc Vol, 2014, 47: 11043–11048
40 Zou Y, Zheng Z W. A robust adaptive RBFNN augmenting backstepping control approach for a model-scaled helicopter. IEEE Trans Contr Syst Technol, 2015, 23: 2344–2352
41 Besnard L, Shtessel Y B, Landrum B. Quadrotor vehicle control via sliding mode controller driven by sliding mode disturbance observer. J Franklin Inst, 2012, 349: 658–684
42 Wang H L, Chen M. Trajectory tracking control for an indoor quadrotor UAV based on the disturbance observer. Trans Inst Measurement Control, 2016, 38: 675–692
43 Dong W, Gu G Y, Zhu X Y, et al. High-performance trajectory tracking control of a quadrotor with disturbance observer. Senss Actuators A-Phys, 2014, 211: 67–77
44 Dinh T X, Ahn K K. Adaptive tracking control of a quadrotor unmanned vehicle. Int J Precis Eng Manuf, 2017, 18: 163–173
45 Hably A, Marchand N. Global stabilization of a four rotor helicopter with bounded inputs. In: Proceedings of the IEEE Conference on Intelligent Robots and Systems, 2007. 129–134
46 Wang Z, Wu Z. Nonlinear attitude control scheme with disturbance observer for flexible spacecrafts. Nonlin Dyn, 2015, 81: 257–264
47 Swaroop D, Hedrick J K, Yip P P, et al. Dynamic surface control for a class of nonlinear systems. IEEE Trans Automat Contr, 2000, 45: 1893–1899
48 Wang D. Neural network-based adaptive dynamic surface control of uncertain nonlinear pure-feedback systems. Int J Robust Nonlin Control, 2011, 21: 527–541